Journal of Ceramic Processing Research. Vol. 26, No. 1, pp. 102~108 (2025)
(Received 15 October 2024, Received in revised form 26 November 2025, Accepted 10 January 2025)
https://doi.org/10.36410/jcpr.2025.26.1.102

J O U R N A L O F
Ceramic Processing Research

Effects of various catalytic promoters on the fast redox reaction of $MgFe_2O_4$ oxygen carrier materials for chemical looping combustion

Jae-Woo Park[a] and Ki-Tae Lee[a,b,c,d,*]
[a]*Division of Advanced Materials Engineering, Jeonbuk National University, Jeonbuk 54896, Republic of Korea*
[b]*Hydrogen and Fuel Cell Research Center, Jeonbuk National University, Jeonbuk 54896, Republic of Korea*
[c]*Department of Energy Storage/Conversion Engineering of Graduate School (BK21 FOUR), Jeonbuk National University, Jeonbuk 54896, Republic of Korea*
[d]*Department of JBNU-KIST Industry-Academia Convergence Research, Jeonbuk National University, Jeonbuk 54896, Republic of Korea*

This study focuses on improving the oxygen transfer properties of a $MgFe_2O_4$ oxygen carrier in chemical looping combustion by introducing the catalytic promoters gadolinium-doped ceria, palladium, and platinum. $MgFe_2O_4$ synthesized by solid-state reactions exhibited reversible redox behavior but suffered from agglomeration and a slow reaction rate. The introduction of palladium and platinum significantly enhanced the oxygen transfer rate in the oxidation and reduction reactions, and the palladium-incorporated composite achieved an oxygen-transfer capacity of 23.40 wt.%, which was similar to that of pure $MgFe_2O_4$ (23.96 wt.%). This improvement can be explained by the participation of PdO as an additional oxygen source. Gadolinium-doped ceria provided microstructural stability and suppressed agglomeration, but the oxygen-transfer rate and capacity were lower due to its oxygen storage property. The palladium-incorporated composite maintained its microstructure after redox cycling, showing excellent redox stability and oxygen transfer properties. These results demonstrate that catalytic promoters such as palladium and platinum not only accelerate the reaction rate, but also improve long-term structural stability, providing important insights into optimizing oxygen carrier materials in chemical looping combustion.

Keywords: Chemical looping combustion, Oxygen carrier material, Redox reaction, Oxygen transfer capacity, Oxygen transfer rate.

Introduction

Fossil fuels remain a substantial part of the global energy mix, and the resulting CO_2 emissions are major contributors to climate change [1]. Various technologies are being studied to reduce these emissions, including chemical looping combustion (CLC) [2, 3]. CLC has the potential to directly capture CO_2 during fuel combustion and is considered an important system of carbon capture and storage [4, 5].

A CLC system comprises two primary and interconnected reactors, an air reactor and a fuel reactor [6]. An oxygen carrier, typically a metal oxide, circulates between these reactors, facilitating the transfer of oxygen required for the process [7]. In the air reactor, the oxygen carrier is oxidized, and in the fuel reactor, the carrier material reacts with the fuel to induce combustion [8]. The reaction in the fuel reactor can be expressed in terms of a typical hydrocarbon fuel by the following equation:

$$C_xH_y + (2x + y/2)MeO \rightarrow xCO_2 + y/2H_2O + (2x + y/2)Me \quad (1)$$

where MeO is the oxidized form of the oxygen carrier, and Me is the reduced form. This is the process by which fuel is supplied with oxygen from the oxygen carrier and combustion occurs, resulting in the production of CO_2 and H_2O. In the air reactor, the reduced oxygen carrier undergoes re-oxidation by reacting with oxygen in the air. This process can be expressed by:

$$Me + 1/2O_2 \rightarrow MeO \quad (2)$$

In this reaction, the oxygen carrier absorbs oxygen from the air and returns to its original oxidized state. The oxidized oxygen carrier then travels back to the fuel reactor, ready to react with the fuel. In this way, CLC efficiently separates CO_2 while minimizing the generation of air pollutants such as NOx as the fuel and air remain isolated and do not interact directly [9].

In a CLC system, the properties of the oxygen carrier are critical to the overall performance and efficiency of the system. The oxygen carrier must meet various requirements, such as a high oxygen transfer capacity,

*Corresponding author:
Tel : +82-63-270-2290
Fax: +82-63-270-2386
E-mail: ktlee71@jbnu.ac.kr

rapid oxidation and reduction rates, physical and chemical stability, and durability [10]. Various metal oxides are being studied as oxygen carriers, including nickel, copper, manganese, and iron-based metal oxides, and each material has unique properties and performance [11-17].

Nickel-based oxide is commonly used in CLC and is characterized by a high oxygen transfer capacity and rapid reaction rate [18]. Nickel has demonstrated excellent catalytic performance and reactivity with various fuels [19]. However, it may be difficult to commercially apply due to its toxicity and high price, and its performance may deteriorate over repeated redox cycles, which may limit its long-term use [20]. Copper-based oxygen carriers are highly reactive even at low temperatures and provide high oxidation/reduction reaction rates [21]. However, the volatility of copper at high temperatures can cause problems with the stability of the material, and the price is relatively high [22]. Manganese-based oxygen carriers, such as Mn_3O_4, offer a moderate oxygen transfer capacity and cost-effective production [23]. During reduction, Mn_3O_4 converts to MnO, which has a high resistance to agglomeration due to suppression of metallic manganese formation under operating conditions. As a result, these oxygen carriers offer excellent thermal stability, rendering them suitable for long-term cyclic processes in high-temperature environments [24].

Iron-based oxygen carriers such as Fe_2O_3 come with several advantages, including a high oxygen transfer capacity, low cost, excellent thermal stability due to a high melting point, and environmental compatibility [25]. However, their reaction kinetics may be slower compared with those of other metal oxides, and performance degradation may occur during long-term cycling [26].

Here, for the first time, we propose $MgFe_2O_4$ spinel oxide as an innovative oxygen carrier for chemical looping hydrogen production [27]. Although $MgFe_2O_4$ undergoes a reversible redox reaction and the reduced $MgFe_2O_4$ (MgO + 2Fe) provides a relatively high oxygen transfer capacity, this spinel oxide suffers slow redox reaction kinetics and agglomeration. To improve the oxygen transfer properties of $MgFe_2O_4$, we incorporated gadolinium-doped ceria ($Ce_{0.9}Gd_{0.1}O_{1.95}$, GDC), palladium, and platinum as catalytic promoters. A systematic investigation of the effects of catalytic promoters on the redox kinetics and oxygen transfer properties of the $MgFe_2O_4$ oxygen carrier materials for CLC was carried out.

Experimental

Powdered $MgFe_2O_4$ was synthesized using a conventional solid-state reaction method. MgO (99.95%, Alfa Aesar, USA) and Fe_2O_3 (99.9%, Alfa Aesar, USA) were mixed in stoichiometric proportions via ball milling in ethanol for 24 h. The resulting mixture was calcined at 1200 °C for 3 h in air. A $MgFe_2O_4$/GDC composite oxygen carrier material was prepared by incorporating 2 wt.% of commercial GDC powder (Kceracell Co. Ltd., Korea) into the $MgFe_2O_4$ matrix via ball milling for 12 h, followed by drying at 80 °C for 24 h.

The $MgFe_2O_4$/Pd and $MgFe_2O_4$/Pt composite oxygen carriers were synthesized through the impregnation of $MgFe_2O_4$ with aqueous palladium and platinum solutions, respectively. A 0.1 M palladium solution and a 0.1 M platinum solution were prepared by dissolving $Pd(NO_3)_2$ (98%, Sigma Aldrich, USA) and $H_2PtCl_6 \cdot 6H_2O$ (ACS reagent, Sigma Aldrich, USA), respectively, in deionized water. The $MgFe_2O_4$ powder was immersed in the prepared solutions at 80 °C under a vacuum environment, followed by heat treatment at 600 °C in an air atmosphere for 1 h to achieve 2 wt.% loading of the respective metals.

Phase analysis was carried out via X-ray diffraction (XRD; MAX-2500, Rigaku, Japan) using a CuKα radiation source. The diffraction patterns were obtained in an angular range of 20° to 80° with a scanning rate of 4°/min, ensuring precise structural analysis.

The microstructure of the $MgFe_2O_4$-based oxygen carrier was examined using high-resolution scanning electron microscopy (SU8230, Hitachi, Japan) both before and after evaluation of its oxygen transport characteristics.

The oxygen transfer properties of the $MgFe_2O_4$-based oxygen carrier during redox reactions within the CLC process were systematically evaluated through thermogravimetric analysis (TGA; TGA-N1000, Shinko, Korea) at an operational temperature of 900 °C. A sample mass of 30 mg was used for the TGA, with a heating rate of 10 °C/min. Redox reactions were induced by supplying air during the oxidation step and a 5% H_2-argon mixture during the reduction step. To prevent gas mixing, the carrier was purged with N_2 for 5 min between each step. The flow rate of all gases used in the analysis was 150 mL/min.

Results and Discussion

Synthesis of $MgFe_2O_4$ via the solid-state method at 1200 °C for 3 h in an air atmosphere was confirmed. The resulting product was a pure single-phase spinel structure without detectable impurities (Fig. 1). Previously, we reported the successful formation of single-phase $MgFe_2O_4$ via the solid-state reaction method [27]. $MgFe_2O_4$ synthesized under calcination conditions below 1200 °C for less than 3 h did not result in a single-phase material, leading to low phase purity. Conversely, calcination temperatures above 1200 °C caused significant grain growth in $MgFe_2O_4$, which could negatively affect its redox behavior. Therefore, the synthesis conditions were optimized to 1200 °C for 3 h to achieve a balance between phase purity and desired

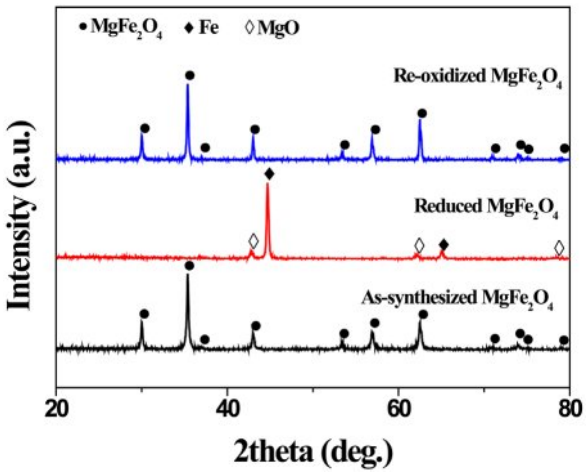

Fig. 1. XRD patterns of as-synthesized $MgFe_2O_4$ and samples after reduction in 5% H_2-argon and re-oxidation in air, respectively, at 900 °C for 2 h.

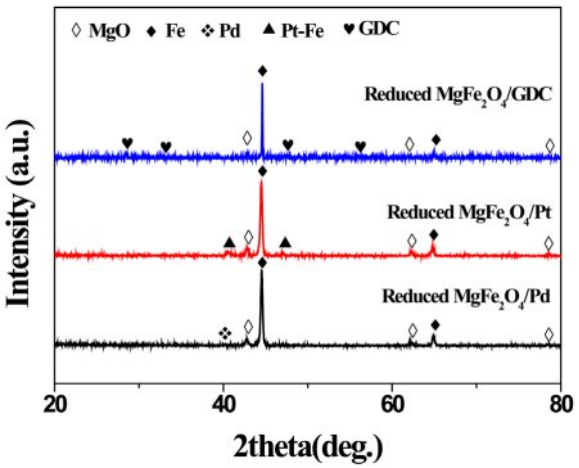

Fig. 3. XRD patterns of $MgFe_2O_4$/GDC, $MgFe_2O_4$/Pd, and $MgFe_2O_4$/Pt composites after reduction in 5% H_2-argon at 900 °C for 2 h.

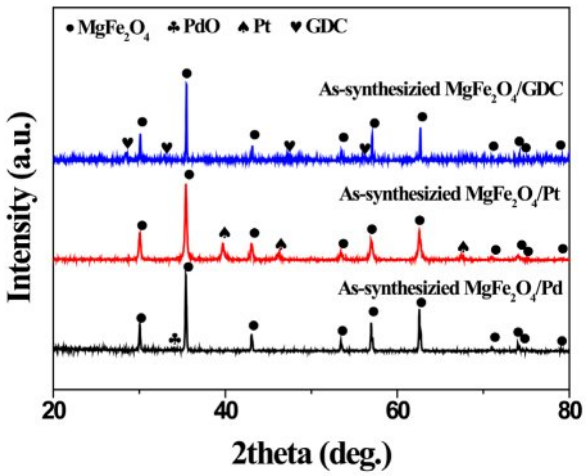

Fig. 2. XRD patterns of as-synthesized $MgFe_2O_4$/GDC (without heat treatment), along with $MgFe_2O_4$/Pd and $MgFe_2O_4$/Pt composites after firing in air at 600 °C for 1 h.

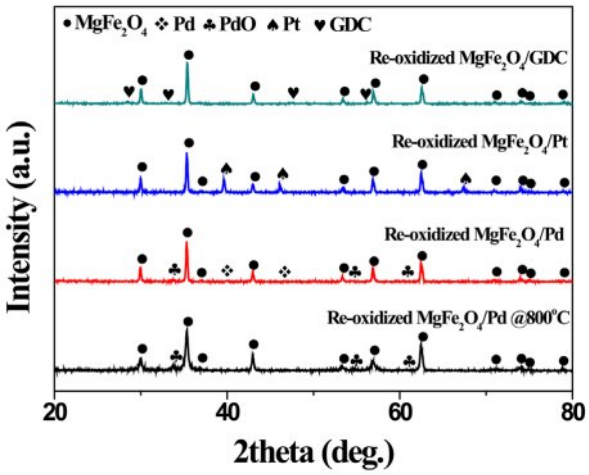

Fig. 4. XRD patterns of $MgFe_2O_4$/GDC, $MgFe_2O_4$/Pd, and $MgFe_2O_4$/Pt composites after re-oxidation in air at 900 °C and 800 °C for 2 h.

material properties. After reduction heat treatment in an 5% H_2-argon atmosphere at 900 °C for 2 h, a $MgFe_2O_4$ powder consisting of metallic iron and MgO phases was observed. Following re-oxidation heat treatment in an air atmosphere at 900 °C for 2 h, the reduced $MgFe_2O_4$ (MgO + 2Fe) successfully reverted to its original structure without passing through secondary phases. A phase analysis provides clear evidence of the reversible redox mechanism of $MgFe_2O_4$ at 900 °C, as described by the following reactions:

$$\text{Reduction: } MgFe_2O_4\ (s) + 3H_2\ (g) \rightarrow MgO\ (s) + 2Fe\ (s) + 3H_2O\ (g) \quad (3)$$

$$\text{Oxidation: } MgO\ (s) + 2Fe\ (s) + 3/2O_2\ (g) \rightarrow MgFe_2O_4\ (s) \quad (4)$$

Figure 2 depicts the XRD patterns of the synthesized $MgFe_2O_4$/GDC, $MgFe_2O_4$/Pd, and $MgFe_2O_4$/Pt composite oxygen carrier materials. The distinct peaks for each component suggest the absence of any interaction between $MgFe_2O_4$ and the incorporated catalytic promoter. Unlike platinum, when palladium was incorporated and heat-treated at 600 °C in air for 1 h, it was observed in the form of its oxide, PdO, rather than its metallic phase.

The XRD patterns of $MgFe_2O_4$/GDC, $MgFe_2O_4$/Pd, and $MgFe_2O_4$/Pt composites after reduction in 5% H_2-argon at 900 °C for 2 h are shown in Fig. 3. $MgFe_2O_4$ undergoes reduction to MgO and metallic iron when exposed to a 5% H_2-argon atmosphere, while GDC and platinum remain in stable phases under these conditions. In contrast, within the as-synthesized $MgFe_2O_4$/Pd composite, palladium exists as PdO, which is reduced to Pd upon reaction with H_2. For the $MgFe_2O_4$/Pt composite, platinum and iron form an alloy, resulting in the presence of a Pt-Fe phase. Formation of an Pt-Fe alloy at 900 °C

has already been reported [28, 29].

Meanwhile, as shown in Fig. 4, when the reduced composite oxygen carrier materials were re-oxidized at 900 °C in air for 2 h, the $MgFe_2O_4$/GDC and $MgFe_2O_4$/Pt composites reverted to their initial as-synthesized phases, whereas in the case of the $MgFe_2O_4$/Pd composite, both PdO and metallic Pd phases were detected. Thermal decomposition of PdO takes place at temperatures above 800 °C [30]. Reduction of PdO initiates within the bulk rather than at the surface, accompanied by hysteresis, and the frequently observed metastable co-existence of Pd and PdO phases can be attributed to kinetic constraints in the oxidation process of the metal [31]. The adsorption of gaseous oxygen on the surface of metallic Pd or PdO is subject to multiple influencing factors, such as particle size, oxygen partial pressure, and the applied polarization conditions [32, 33]. In fact, upon re-oxidation at 800 °C, Pd was not detected, as shown in Fig. 4. Based on the phase analysis in Figs. 3 and 4, the redox mechanism of the $MgFe_2O_4$/Pd composite can be described as follows.

$$\text{Reduction: } MgFe_2O_4\ (s) + PdO\ (s) + 4H_2\ (g) \rightarrow MgO\ (s) + 2Fe\ (s) + Pd(s) + 4H_2O\ (g) \quad (5)$$

$$\text{Oxidation: } MgO\ (s) + 2Fe\ (s) + Pd(s) + 2O_2\ (g) \rightarrow MgFe_2O_4\ (s) + (1\text{-}x)Pd\ (s) + xPdO\ (s) + (1\text{-}x)/2O_2\ (g) \quad (6)$$

Redox cycle curves of the $MgFe_2O_4$, $MgFe_2O_4$/GDC, $MgFe_2O_4$/Pd, and $MgFe_2O_4$/Pt composite oxygen carrier materials during three redox cycles at 900 °C are shown in Fig. 5. During reduction reactions, as oxygen is released from the oxygen carrier and reacts with H_2, the mass of the sample decreases. In the subsequent oxidation reaction, oxygen from the air combines with the reduced oxygen carrier, resulting in an increase in mass. The mass fluctuations observed during the N_2 purge between redox reactions may be caused by inaccuracies in gas-flow rates due to equipment limitations or differences

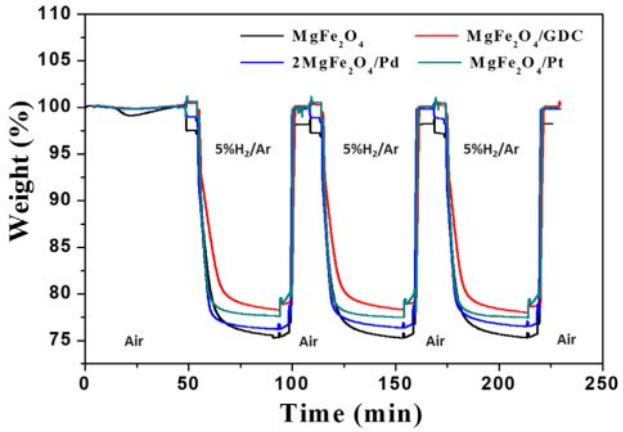

Fig. 5. Redox cycle curves of $MgFe_2O_4$, $MgFe_2O_4$/GDC, $MgFe_2O_4$/Pd, and $MgFe_2O_4$/Pt composite oxygen carrier materials at 900 °C.

Table 1. Oxygen transfer capacities and maximum oxygen transfer rates of $MgFe_2O_4$, $MgFe_2O_4$/GDC, $MgFe_2O_4$/Pd, and $MgFe_2O_4$/Pt composites during the first redox cycle at 900 °C.

Sample	Oxygen transfer capacity (wt.%)	Maximum oxygen transfer rate (mmol O_2/g/s)	
		Oxidation	Reduction
$MgFe_2O_4$	23.96	0.0158	0.0068
$MgFe_2O_4$/GDC	21.54	0.0124	0.0067
$MgFe_2O_4$/Pd	23.40	0.0194	0.0108
$MgFe_2O_4$/Pt	21.39	0.0199	0.0106

in heat-transfer rates. The weight gain during oxidation matched the weight loss during reduction, confirming the reversibility of the redox reaction. The reversibility of this redox reaction is further supported by a phase analysis, as demonstrated in Figs. 1, 2, 3, and 4.

The oxygen transfer capacity can be determined by:

$$(m_{ox} - m_{red})/m_{ox} \quad (7)$$

where m_{ox} represents the fully oxidized mass and m_{red} represents the fully reduced mass. The oxygen transfer capacity of the first cycle, calculated from the data shown in Fig. 5, is presented in Table 1. The experimentally determined oxygen transfer capacity of $MgFe_2O_4$ was 23.96 wt.%, closely matching the theoretical value of 24.0 wt.%. Because catalytic promoters do not directly engage in oxygen transfer reactions, the incorporation of catalytic promoters such as GDC or platinum resulted in a decrease in oxygen transfer capacity. However, the $MgFe_2O_4$/Pd composite exhibited an oxygen transfer capacity of 23.40 wt.%, which is comparable to that of $MgFe_2O_4$ alone. As indicated in Fig. 2 and according to the redox mechanism of the $MgFe_2O_4$/Pd composite based on eqs. (5) and (6), palladium exists as PdO in the as-synthesized $MgFe_2O_4$/Pd composite, enabling PdO to serve as an oxygen transfer material.

The oxygen transfer rate, the amount of oxygen consumed per unit time and mass, can be derived by differentiating the TGA data. Fig. 6 shows the variation in oxygen transfer rate, calculated from the slope of the mass-change curve during the first redox cycle. Maximum oxygen transfer rate values are presented in Table 1. The oxygen transfer rate during oxidation was significantly higher than that of the reduction reaction. Similar redox kinetics were observed with iron-based ore [34]. The activation energy for the oxidation reaction was 16.70 kJ/mol, whereas the activation energy for the reduction reaction was 42 kJ/mol. The oxygen transfer rate during oxidation of the iron-based ore was therefore much higher than that of the reduction reaction.

The primary reason for incorporating a catalytic promoter is to enhance the oxygen transfer rate, even if it slightly reduces the oxygen transfer capacity. In contrast,

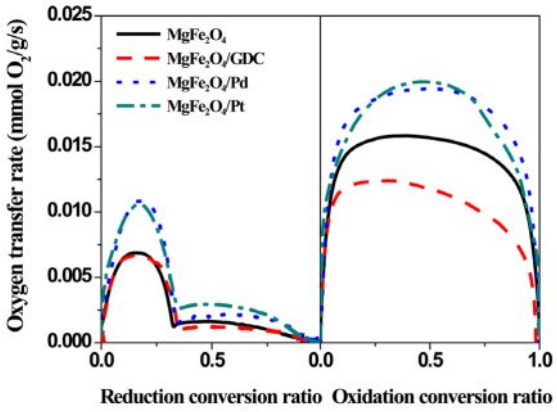

Fig. 6. Variation of oxygen transfer rates of $MgFe_2O_4$, $MgFe_2O_4$/GDC, $MgFe_2O_4$/Pd, and $MgFe_2O_4$/Pt composite oxygen carrier materials during the first redox cycle at 900 °C.

during the reduction process, the $MgFe_2O_4$ incorporating GDC as a catalyst exhibited an oxygen transfer rate similar to that of pristine $MgFe_2O_4$, indicating that GDC is ineffective catalyst for the reduction reaction. During oxidation, the presence of GDC had an adverse impact on the oxygen transfer rate. This behavior can be explained by the oxygen storage capacity of GDC, which is known for its ability to store oxygen through the presence of oxygen vacancies [35]. During the oxidation reaction, oxygen molecules adsorbed at oxygen vacancies are preferentially incorporated into the GDC lattice, reflecting oxygen storage rather than participation in the reaction. The oxygen transfer rates of the $MgFe_2O_4$/GDC composite during the oxidation process were lower than those of pristine $MgFe_2O_4$. A similar trend was observed in $MgMnO_3$/GDC composite oxygen carrier

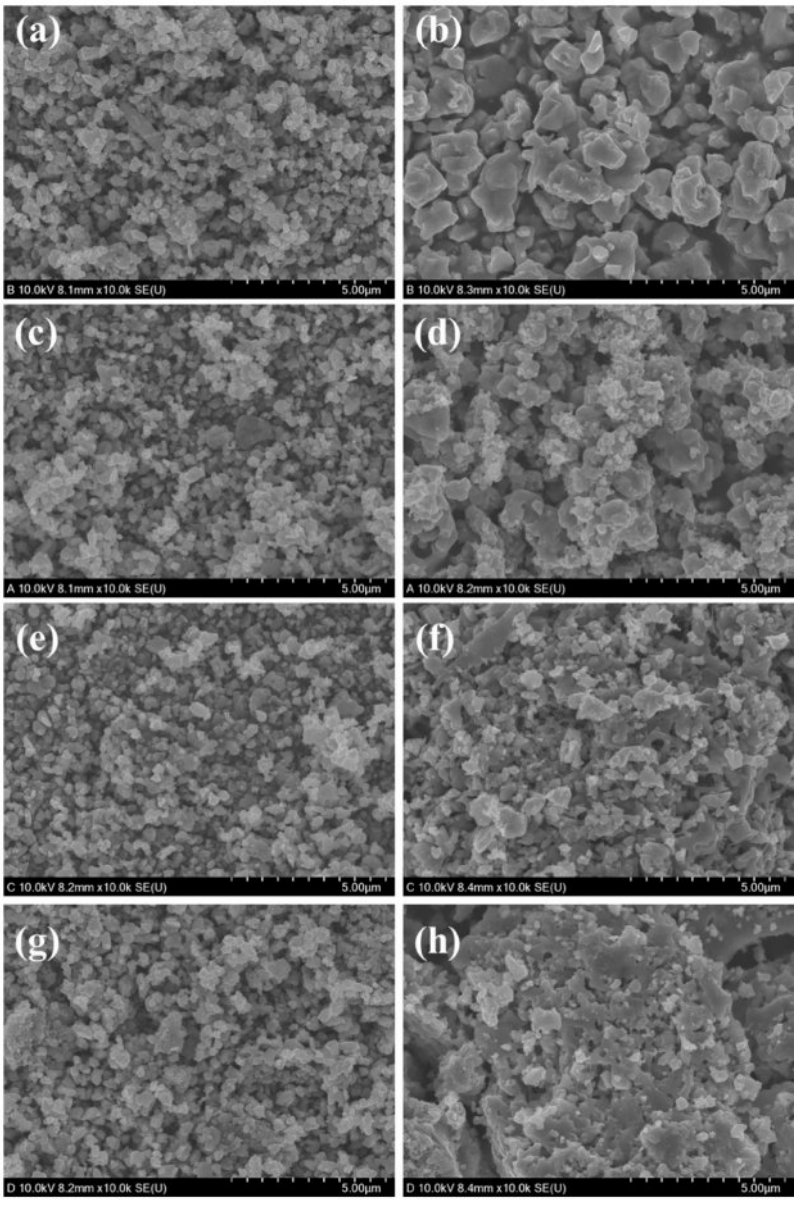

Fig. 7. High-resolution scanning electron microscope images of (a, b) $MgFe_2O_4$, (c, d) $MgFe_2O_4$/GDC, (e, f) $MgFe_2O_4$/Pd, and (g, h) $MgFe_2O_4$/Pt composite oxygen carrier materials: (a, c, e, g) before and (b, d, f, h) after three redox cycles.

materials [16]. However, since oxygen adsorption can be influenced by the surface morphology, controlling the shape or dispersion of GDC could potentially minimize the impact associated with its oxygen storage properties.

In contrast to the addition of GDC, the incorporation of platinum and palladium resulted in a substantial enhancement of the oxygen transfer rate, which was notably higher during both oxidation and reduction. Platinum and palladium are widely recognized as prominent catalytic materials in chemical reactions [36-38]. In particular, they are key components of electrode catalysts in fuel cells, where they play a critical role in facilitating oxygen and hydrogen redox reactions [39-41]. Additionally, the low activation energy of platinum and palladium as promoters for the oxidation of H_2 has been well-documented in the literature [42, 43]. Meanwhile, the redox reactions of oxygen carrier materials proceed through several sequential steps, including gas-phase diffusion, surface chemisorption, charge transfer, and bulk diffusion, with any of these stages potentially acting as the rate-limiting step of the overall process. Catalytic promoters such as platinum and palladium enhance the surface adsorption capacity for reaction gases such as H_2 and O_2. The observed improvement in the oxygen transfer rate of $MgFe_2O_4$ upon incorporation of platinum and palladium is primarily attributable to increased surface adsorption of the reaction gases, H_2 and O_2.

The microstructures of $MgFe_2O_4$, $MgFe_2O_4$/GDC, $MgFe_2O_4$/Pd, and $MgFe_2O_4$/Pt composite oxygen carrier materials, both before cycling and after three redox cycles at 900 °C, are shown in Fig. 7. The pristine $MgFe_2O_4$ sample exhibited significant agglomeration and grain growth after the redox cycles (Fig. 7a and b). However, the presence of well-dispersed catalytic promoter particles in the composite materials (Fig. 7c-h) effectively inhibited the aggregation of $MgFe_2O_4$ particles. Notably, the palladium-incorporated composite retained its initial microstructure most effectively even after the redox cycles (Figs. 7e and f). In general, agglomeration reduces the specific surface area of the oxygen carrier, which significantly diminishes its reactivity due to a substantial decrease in the number of available active sites. From this perspective, catalytic promoters such as GDC, platinum, and palladium can enhance oxygen transfer not only by accelerating reaction kinetics, but by providing microstructural stability through the suppression of agglomeration during redox cycles.

Conclusions

In this study, enhancement of the oxygen transfer properties of $MgFe_2O_4$ for CLC through the incorporation of catalytic promoters such as GDC, platinum, and palladium was investigated. In the case of GDC, both the oxygen transfer capacity and the oxygen transfer rate during the oxidation reaction decreased due to its oxygen storage properties, trapping oxygen in the GDC lattice rather than allowing it to directly participate in redox reactions. However, the addition of platinum and palladium significantly enhanced oxygen transfer during both oxidation and reduction by increasing surface adsorption of the reactant gases (H_2 and O_2). The palladium-incorporated composite maintained an oxygen transfer capacity comparable to that of pure $MgFe_2O_4$ due to PdO's participation in the process, indicating that PdO serves as an additional source of oxygen. The catalytic promoters also improved overall microstructural stability by suppressing agglomeration during redox cycling. Among the studied composites, the palladium-incorporated material exhibited the best retention of its initial microstructure, showcasing excellent redox stability and enhanced oxygen transfer properties. These findings demonstrate that catalytic promoters such as platinum and palladium not only enhance reaction kinetics, but improve long-term durability by stabilizing the microstructure. While platinum and palladium are indeed expensive materials, cost-efficient alternatives include strategies such as reducing particle size to maintain the same specific surface area with a lower overall catalyst loading or alloying platinum and palladium with more cost-effective metals. These approaches could provide both effective and economically sustainable solutions.

Acknowledgements

This work was supported by Korea Institute of Energy Technology Evaluation and Planning (KETEP) grant funded by the Korea government (MOTIE) (20213030040110). This work was supported by the Commercialization Promotion Agency for R&D Outcomes (COMPA) grant funded by the Korean Government (Ministry of Science and ICT, 2023) (RS-2023-00304743). This research was supported by Regional Innovation Strategy (RIS) through the National Research Foundation (NRF) funded by the Ministry of Education (MOE) (2023RIS-008).

CRediT Authorship Contribution Statement

Jae-Woo Park: Investigation, Data curation, Formal analysis, Validation, Writing - original draft. **Ki-Tae Lee**: Conceptualization, Funding acquisition, Investigation, Methodology, Supervision, Validation, Writing - original draft, Writing - review and editing.

Conflict of Interest Statement

The authors have no conflicts of interest to declare. All co-authors have seen and agree with the contents of the manuscript and there is no financial interest to report. We certify that the submission is original work and is not under review at any other publication.

Data Availability Statement

The data that support the findings of this study are available from the corresponding author upon reasonable request.

References

1. S. Daneshmand-Jahromi, M.H. Sedghkerdar, and N. Mahinpey, Fuel 341 (2023) 127626.
2. T. Czakiert, J. Krzywanski, A. Zylka, and W. Nowak, Energies 15 (2022) 1563.
3. A. Lyngfelt, Energy Fuels 34 (2020) 9077-9093.
4. S. Abuelgasim, W. Wang, and A. Abdalazeez, Sci. Total Environ. 764 (2021) 142892.
5. S. Saqline, Z.Y. Chua, and W. Liu, Energy Conv. Manag. 244 (2021) 114455.
6. A. Abdalla, M. Mohamedali, and N. Mahinpey, Catal. Today 407 (2023) 21-51.
7. R.A. Newby, D.L. Keairns, and R.W. Stevens, Appl. Energy 345 (2023) 121293.
8. M. Qasim, M. Ayoub, N.A. Ghazali, A. Aqsha, and M. Ameen, Ind. Eng. Chem. Res. 60 (2021) 8621-8641.
9. Y. De Vos, M. Jacobs, P. Van Der Voort, I. Van Driessche, F. Snijkers, and A. Verberckmoes, Catalysts 10 (2020) 926.
10. F. Liu, J. Liu, and Y. Yang, Energy Fuels 36 (2022) 9373-9384.
11. J. Zhang, H. Zhang, N. Yuan, L. Meng, C. Geng, and H. Bai, Fuel Process. Technol. 229 (2022) 107181.
12. G. Liu and G. Lisak, Fuel 342 (2023) 127828.
13. J.H. Hwang, J.I. Baek, H.J. Ryu, J.M. Sohn, and K.-T. Lee, Fuel 231 (2018) 290-296.
14. Z. Ma, G. Liu, Y. Lu, J. Wang, and H. Zhang, Fuel Process. Technol. 224 (2021) 107030.
15. J.H. Hwang and K.-T. Lee, J. Ceram. Process. Res. 19[5] (2018) 372-377.
16. J.H. Hwang and K.-T. Lee, J. Ceram. Process. Res. 20[1] (2019) 18-23.
17. J.H. Hwang and K.-T. Lee, J. Ceram. Process. Res. 21[2] (2020) 148-156.
18. M.H. Sedghkerdar, D. Karami, and N. Mahinpey, Fuel 274 (2020) 117838.
19. Y. Yuan, X. Dong, and L. Ricardez-Sandoval, Fuel Process. Technol. 229 (2022) 107172.
20. A. Abdalla, M.M. Tijani, M. Mohamedali, and N. Mahinpey, J. Environ. Chem. Eng. 10 (2022) 106945.
21. C. Zheng, M. Su, and H. Zhao, Fuel 334 (2023) 126720.
22. A. Cabello, A. Abad, T. Mendiara, M.T. Izquierdo, and L.F. de Diego, Chem. Eng. J. 455 (2023) 140484.
23. K. Idziak, T. Czakiert, J. Krzywanski, A. Zylka, M. Kozlowska, and W. Nowak, Fuel 268 (2020) 117245.
24. T.R. Costa, P. Gayán, A. Abad, F. García-Labiano, L.F. de Diego, D.M.A. Melo, and J. Adánez, Fuel Process. Technol. 178 (2018) 236-250.
25. W.-H. Chen, K.-H. Chen, A.T. Ubando, W.-J. Lee, and M.-H. Chio, Chem. Eng. J. 426 (2021) 130834.
26. Y. Guan, Y. Liu, X. Lin, B. Wang, and Q. Lyu, Energy Fuels 36 (2022) 13956-13984.
27. J.H. Hwang and K.-T. Lee, J. Ceram. Process. Res. 21[1] (2020) 57-63.
28. P. Vlaic and E. Burzo, J. Optoelectron. Adv. Mater. 12 (2010) 1114-1124.
29. Y. Nose, A. Kushida, T. Ikeda, H. Nakajima, K. Tanaka, and H. Numakura, Mater. Trans. 44 (2003) 2723-2731.
30. H. Zhang, J. Gromek, G.W. Fernando, S. Boorse, and H.L. Marcus, J. Phase Equilibria 23 (2002) 246-248.
31. M.M. Wolf, H. Zhu, W.H. Green, and G.S. Jackson, Appl. Catal. A Gen. 244 (2003) 323-340.
32. F. Wang, A. Wang, J. Chen, B. Chi, J. Pu, and L. Jian, Int. J. Hydrogen Energy 39 (2014) 14421-14427.
33. S. Penner, P. Bera, S. Pedersen, L.T. Ngo, J.J.W. Harris, and C.T. Campbell, J. Phys. Chem. B, 110 (2006) 24577-24584.
34. E. Ksepko, P. Babinski, A. Evdou, and L. Nalbandian, J. Therm. Anal. Calorim. 124 (2016) 137-150.
35. C. Sun, H. Li, and L. Chen, Energy Environ. Sci. 5 (2012) 8475-8505.
36. J. Wisniak, Educ. Quím. 21[1] (2010) 60-69.
37. H. An, G.-H. An, and H.-J. Ahn, J. Ceram. Process. Res. 16[2] (2015) 208-212.
38. D. Suastiyantia, M. Wijaya, and B.G. Pandita J. Ceram. Process. Res. 25[2] (2024) 261-267.
39. X. Yang, L. Lin, X. Guo, and S. Zhang, Small 20 (2024) 2404000.
40. J.H. Koo and K.-T. Lee, J. Ceram. Process. Res. 17[9] (2016) 965-968.
41. S. Suthirakun, T. Sarakonsri, S. Aukkaravittayapun, and T. Vilaithong, J. Ceram. Process. Res. 10[4] (2009) 502-506.
42. J. Durst, C. Simon, F. Hasché, and H.A. Gasteiger, J. Electrochem. Soc. 162 (2015) F190-F203.
43. L. Liu, F. Zhou, L. Wang, X. Qi, F. Shi, and Y. Deng, J. Catal. 274 (2010) 1-10.